A Plumbline Constraint for the Rational Function Lens Distortion Model

David Claus
University of Oxford
dclaus@robots.ox.ac.uk

Andrew W. Fitzgibbon
Microsoft Research
awf@microsoft.com

Abstract

The recently introduced Rational Function (RF) model permits a linear solution of epipolar geometry and lens distortion from image correspondences for a very general class of lenses. In this paper we show that the model also permits a very elegant form of the plumbline constraint which allows uncalibrated correction of lens distortion from a single image containing lines known to be straight in the world. We show how this may be expressed as a factorization problem, and discuss its behaviour with noisy data. We also introduce a simple reduced parametrization of the RF model which again models a range of existing lenses. Because the RF model provides a very simple form for the distorted lines, nonlinear minimization can compute the Sampson distance to the distorted lines, allowing fast and accurate estimation of the RF model even from noisy images.

1 Introduction

The "Rational Function" (RF) model for lens distortion in general cameras was recently introduced to computer vision [7, 12, 24]. In [7], we showed that the model allows linear estimation of distortion parameters for a range of highly distorted cameras in two cases: a calibration grid in unknown position relative to the camera; and two-view structure and motion recovery. However, the latter was shown to be unstable in many cases, so is not yet a useful calibration strategy. On the other hand, in many real-world situations sequences have been shot without calibration grids, and distortion must be corrected. We show in this paper how a plumbline constraint can be implemented using the RF model. This differs from previous plumbline work in two ways: first, a factorization-based algorithm can be formulated to estimate the distortion; second, nonlinear refinement of the distortion can be easily implemented to minimize a good approximation of geometric distance in the image plane. While this was possible with previous models, the simplicity of the mapping in this case appears to lead to fast and efficient convergence of the nonlinear algorithm over a range of starting positions.

The main contributions of this paper are four. 1. We show quantitatively how the RF model compares to a number of existing models for large-distortion lenses. 2. We show that the image of a straight line under the RF model is a conic, and that a simple factorization algorithm can be formed which simultaneously estimates distortion and the parameters of the 3D lines. 3. We provide a parametrization of the rational function model based on the physical properties of a camera. 4. We present a robust method for estimating the model parameters using detected images of straight lines.

BMVC 2005 doi:10.5244/C.19.10

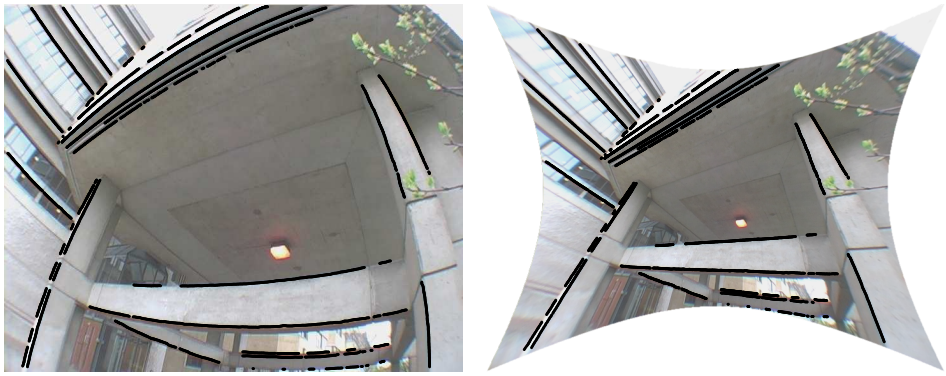

Figure 1: Image rectified using the rational function model. Edgels along 22 straight lines in the real world were detected in this single frame of video and the plumbline constraint used to compute the distortion parameters.

2 Background

There is a wealth of literature on the subject of camera calibration; in this section we first summarize methods of general camera calibration and then outline the models employed for nonlinear distortion.

As described in [18, 22], calibration of a camera amounts to determining the 3D ray from which each pixel samples. This process can be separated into two transformations. The first is a rotation $\mathtt{R}$ and translation $\mathbf{t}$ between the world and camera coordinate systems, referred to as the external calibration. The second is a projection from world points (x,y,z) in $\mathbb{R}^3$ to image pixels (i,j) in $\mathbb{R}^2$. For a central pinhole camera this mapping is represented by

$$(i,j) = \pi\left(\mathtt{K}\left[\mathtt{R} \mid \mathbf{t}\right](x,y,z,1)^\top\right), \tag{1}$$

where the 3D-to-2D perspective projection function is defined as $\pi(x,y,z) = (x/z, y/z)$. The matrix $\mathtt{K}$ represents the internal calibration parameters of the camera:

$$\mathtt{K} = \begin{bmatrix} f & s & u_0 \\ 0 & af & v_0 \\ 0 & 0 & 1 \end{bmatrix} \qquad \begin{cases} f \text{ is focal length;} \\ (u_0, v_0) \text{ is principal point;} \\ a \text{ is aspect ratio; } s \text{ is skew} \end{cases} \tag{2}$$

By defining the world coordinate system to be coincident with the camera center the pinhole projection reduces to $(i,j) = \pi(\mathtt{KR}(x,y,z)^\top)$. Thus, for a perspective camera, the mapping from image pixels to 3D rays $\mathbf{d}(i,j)$ in $\mathbb{R}^3$ can be expressed as:

$$\mathbf{d}(i,j) = \begin{pmatrix} B_{11}i + B_{12}j + B_{13}1 \\ B_{21}i + B_{22}j + B_{23}1 \\ B_{31}i + B_{32}j + B_{33}1 \end{pmatrix} = \mathtt{B}\begin{pmatrix} i \\ j \\ 1 \end{pmatrix}, \tag{3}$$

where the 3×3 matrix $\mathtt{B} = \mathtt{R}^\top \mathtt{K}^{-1}$, and $\mathtt{R}$ is often chosen to be the identity. For high quality lenses, the pinhole projection model accurately reflects the physics of the camera.

However, video and consumer digital cameras often exhibit significant levels of nonlinear distortion. Techniques for modelling this distortion are detailed in §3.2, but they can be separated into radial polynomial [3, 14, 26], radial field of view [1, 8], and general techniques [18, 22].

Previously, it has been necessary to use specific lens-specific models depending on the level of distortion expected, particularly in the case of fish-eye [8] or catadioptric [16] cameras. The Rational Function (RF) model [7, 24] is an extension of the recent work on catadioptric and general [11, 22] cameras that models nonlinear distortion via mapping to a higher dimensional space where the distortion can be expressed linearly (see §3).

There are several classes of known information that can be exploited to calibrate a camera. The first is to use known correspondences between feature points in one or more images, and the world 3D points. This is typically done using a checkerboard or a calibration grid of dots where corners or dot centres can be reliably located [3, 14, 26]. A second class of calibration techniques relies upon geometric invariants within the image (such as parallel lines [2, 6] or spheres [17]), rather than their world coordinates. The third family of calibration methods is termed auto-calibration as it relies solely on detecting static points within a scene [9, 21, 27].

This paper fits into the second category, where straight lines in the world are used to determine the distortion parameters. This *plumbline* technique was first mooted by [4], and has been applied to various distortion models [8, 21, 23]. We will show that the rational function model images straight lines as conics, and this permits an elegant factorization of the conics into the camera calibration and the equations of the straight lines.

We now proceed with the explanation of the rational function model, its efficient parametrization, and application of the plumbline constraints.

3 Rational Function Model

The Rational Function (RF) model has been recently introduced to computer vision [7]. Although prefigured in earlier work [12, 24], reference [7] appears to be the first to lay out the epipolar geometry induced by the model, and to introduce linear algorithms for some calibration problems. In this section we briefly outline the model and compare it with other models for radial lens distortion.

The pinhole camera model (3) maps image pixels to 3D rays via a vector of linear polynomials in (i, j). Because it is linear in image coordinates it is unable to model the non-linear distortion present in video optics and low-cost wide angle lenses. The rational function model handles this lens distortion by permitting i and j to appear in higher order polynomials, in particular quadratic:

$$\mathbf{d}(i,j) = \begin{pmatrix} A_{11}i^2 + A_{12}ij + A_{13}j^2 + A_{14}i + A_{15}j + A_{16} \\ A_{21}i^2 + A_{22}ij + A_{23}j^2 + A_{24}i + A_{25}j + A_{26} \\ A_{31}i^2 + A_{32}ij + A_{33}j^2 + A_{34}i + A_{35}j + A_{36} \end{pmatrix}. \tag{4}$$

This model may be written as a linear combination of the distortion parameters, in a 3×6 matrix `A` (analogous to `B` above), and a 6-vector χ of monomials in i and j. Define χ as the "lifting" of image point (i, j) to a six dimensional space

$$\chi(i,j) = [i^2,\ ij,\ j^2,\ i,\ j,\ 1]^\top \tag{5}$$

The imaging model (4) may then be written

$$\mathbf{d}(i,j) = \mathtt{A}\chi(i,j) \tag{6}$$

where $\mathbf{d}$ is a vector in camera coordinates representing the ray direction along which pixel (i,j) samples. Undistorted image coordinates (p,q) are computed by the perspective projection of $\mathbf{d}$:

$$(p,q) = \left(\frac{A_1^\top \chi(i,j)}{A_3^\top \chi(i,j)}, \frac{A_2^\top \chi(i,j)}{A_3^\top \chi(i,j)}\right) \tag{7}$$

where the rows of $\mathtt{A}$ are denoted by $A_{1..3}^\top$. We see that the mapping $(i,j) \to (p,q)$ is a quotient of polynomials, or *rational function*, in the image coordinates.

Back-projecting an image point to a ray in 3D space is done by simply lifting the point and applying (6). To *project* a 3D point (expressed in camera coordinates as ray $\mathbf{d} = (d_1, d_2, d_3)^\top$) into the image plane we must intersect the pair of conics

$$\begin{aligned}(d_1 A_3 - d_3 A_1)^\top \chi(i,j) = 0 \\ (d_2 A_3 - d_3 A_2)^\top \chi(i,j) = 0\end{aligned} \tag{8}$$

yielding up to four possible image locations (i,j), of which the correct one can easily be determined. Here we have expressed the calibration matrix $\mathtt{A}$ as three conics $A_{1..3}^\top$ as described in §3.1.

3.1 Physical camera properties

A linear method for computing a general $\mathtt{A}$ using a calibration grid was detailed in [7]. This section examines the relationship between $\mathtt{A}$ and the physical properties of a camera.

As mentioned above for the pinhole camera, we can recover the internal calibration by defining the world coordinate origin at the camera centre. It can be shown [7] that such an internal calibration can always be expressed in the canonical form:

$$\mathtt{A} = \begin{bmatrix} \times & \times & \times & \times & 0 & 0 \\ \times & \times & \times & 0 & \times & 0 \\ \times & \times & \times & \times & \times & \times \end{bmatrix}. \tag{9}$$

Denote the rows of $\mathtt{A}$ by $A_{1..3}^\top$ and note that each row may be identified with a conic in the image plane. The conic described by the first row of $\mathtt{A}$ is the set of image points whose world ray's $d_1 = 0$; that is, the conic A_1 is the image of the world YZ plane. Similarly, conic A_2 is the image of the world XZ plane. For a camera with zero skew and square pixels the tangents to these two conics at the image centre are perpendicular. Points at infinity on the image plane are imaged onto the conic A_3, which is visible in the image only for cameras with a field of view greater than 180° (see Figure 3).

We can further constrain the form of $\mathtt{A}$ through knowledge of camera and lens properties. Each conic will be a circle if the pixels are square and the image plane is parallel to the coordinate axes. Furthermore, the centre of A_1 lies along the Y axis, A_2 on the X axis, and A_3 at the origin. The rational function model can then be expressed in terms of new

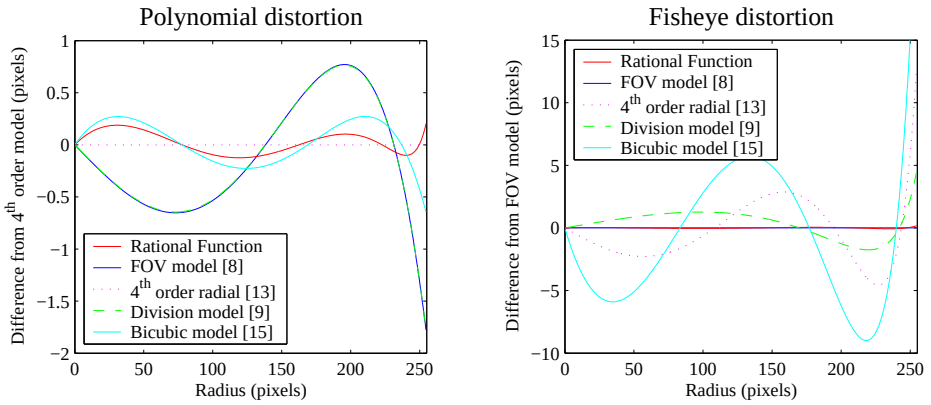

Figure 2: Comparison of the rational function model with existing lens distortion models. *Left* Moderate polynomial distortion corresponding to a standard consumer lens. All models are compared to the 4^{th} order fit as it seems to be the most commonly used. Note that for low distortion the FOV model collapses to the division model. *Right* Fish-eye lens distortion is fit best by the FOV model, so it is taken as ground truth. The rational function model provides a very close approximation, and can be fit linearly.

geometric parameters (a,b,w,h,ω) as:

$$A_1: \quad \left(i-(b+\tfrac{w}{2})\right)^2+\frac{1}{a^2}\left(j-\tfrac{h}{2}\right)^2=b^2 \qquad \text{(image of the world } YZ \text{ plane)}$$

$$A_2: \quad \left(i-\tfrac{w}{2}\right)^2+\frac{1}{a^2}\left(j-(b+\tfrac{h}{2})\right)^2=b^2 \qquad \text{(image of the world } XZ \text{ plane)}$$

$$A_3: \quad \left(i-\tfrac{w}{2}\right)^2+\frac{\left(j-\frac{h}{2}\right)^2}{a^2}=\frac{(wa)^2+h^2}{4\omega^2a^2} \qquad \text{(image of the world } XY \text{ plane horizon)}$$

where (i,j) are image coordinates, with the image origin in the top-left; w,h are the width and height of the image in pixels and a is the pixel aspect ratio. Two important shape parameters for the lens are ω, representing the field of view; and b, which represents the diameters of the first two conics. The image dimensions are known, so this parametrization reduces the number of unknowns in $\mathtt{A}$ from 14 (for the canonical form) to 3. The pixel aspect ratio is typically known, (*e.g.* $a=576/720\times 4/3=1.0667$), and the conic radius can be set to a large number (*e.g.* 2×10^7). The field of view parameter can also be reasonably approximated for most lenses (*e.g.* $\omega=0$ for pinhole, 0.5 for fish-eye).

3.2 Distortion model comparison

There are many existing models for nonlinear distortion in camera lenses. In addition to being easy to fit and elegantly representing the distortion observed in true images, this section shows how accurately the RF model can approximate existing models.

Lens distortion can be separated into radial and tangential components where the former is experimentally observed to be more significant [20]. This radial distortion is often approximated by the first few even terms of a Taylor series expansion [13, 14, 26], and has

been shown to achieve high accuracy [3]. We selected a fourth (and second) order polynomial and measured typical values for a lens with moderate distortion (Nikon Coolpix). The 4^{th} order radial model was then used to generate a set of distorted image coordinates. Figure 2 shows the fitting error of several alternative models on this synthetic data. The rational function model provides the closest approximation to the 4^{th} order radial model, with a maximum difference less than 0.25 pixels.

For fish-eye and other lenses with extreme distortion it may be necessary to include many higher order terms of the Taylor expansion. A more concise representation is obtained by parameterizing by the field of view (FOV), since these lenses are designed so that the image resolution is roughly proportional to the distance from the image centre [8]. Figure 2 also provides a comparison against this FOV model (synthetic data was generated based on the observed parameters of a Raynox *0.3X* fish-eye adapter fitted to a Canon *XM2* digital camcorder). Once again, the rational function model provides an extremely close approximation while the polynomial models vary widely. Both the details of the models and a comparison against ground truth for a real lens are given in [7]. For all of these tests the models were fit to the data using non-linear optimization including overall scaling and translation parameters in addition to the model parameters.

It is important to bear in mind that all of these models are merely approximations to a camera's true distortion function; we would like to select the model which most accurately fits this underlying (unknown, and potentially highly complex) function with the least number of parameters. However, the ability of RF to fit these rather different models provides some confidence in its general-purpose applicability.

4 Plumb-line constraints

In sequences where there are straight lines in the scene, it is desirable to be able to impose the constraint that the back-projections of their images are straight. In order to do so, we first investigate the form of their image projections under the RF model. Given these forms, we will be in a position to present a factorization-based algorithm for their reconstruction.

A line in the scene forms a plane with the origin of camera coordinates, and is imaged to the set of $\mathbf{d}$ in that plane. This yields the line equation $\mathbf{l}^\top \mathbf{d} = 0$ which, in terms of image points (i, j) becomes

$$\mathbf{l}^\top \mathtt{A} \chi = 0 \Longleftrightarrow \theta^\top \chi = 0, \tag{10}$$

where $\theta = \mathtt{A}^\top \mathbf{l} = (A_{xx}, A_{xy}, A_{yy}, A_x, A_y, A_0)^\top$ are the parameters of a conic in image coordinates (i, j) and χ is given by (5). Here we observe the important property that lines in the world go to conics under the rational function model. The task of calibration is then to find an $\mathtt{A}$ which will map these conics in the distorted image back to straight lines.

By fitting a conic to the image of the line, we obtain parameters θ, and thus the constraint

$$\theta = \mathtt{A}^\top \mathbf{l} \tag{11}$$

for unknown $\mathtt{A}$ and $\mathbf{l}$. The equality is exact (*i.e.* not just up to scale) as any scale factor is

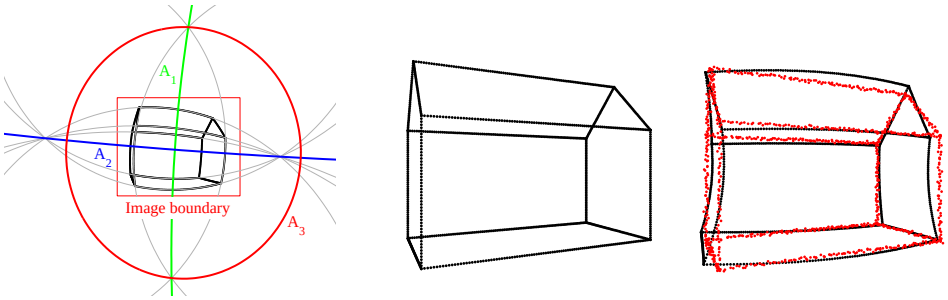

Figure 3: Plumbline constraints on a single synthetic image. *Left* Conics corresponding to parallel lines intersect; lines which are also parallel to the image plane intersect on A_3, the image plane horizon. *Top* With low noise the calibration $\mathtt{A}$ can be recovered via factorization of the conic matrix $\mathtt{C}$. *Bottom* At a noise level of 0.01 pixels the linear factorization solution (black points) begins to break down, but the nonlinear method (red points) continues to accurately recover the rectification (noise level of 2 pixels shown).

included in $\mathbf{l}$. Collecting L such constraints, we obtain

$$\underbrace{[\theta_1 \mid \ldots \mid \theta_L]}_{6\times L} = \underbrace{\mathtt{A}^\top}_{6\times 3}\underbrace{[\mathbf{l}_1 \mid \ldots \mid \mathbf{l}_L]}_{3\times L} \tag{12}$$

$$\mathtt{C} = \mathtt{A}^\top \mathtt{L} \tag{13}$$

so the matrix of conic parameters $\mathtt{C}$ is of rank no greater than 3. Therefore $\mathtt{A}$ can be computed up to a homography by factorization: if $\mathtt{USV}^\top = \mathtt{C}$ is the SVD of $\mathtt{C}$, then $\mathtt{A} = \mathtt{S}_{(1:3,1:3)}\mathtt{U}_{(:,1:3)}{}^\top$ is one member of the equivalence class of solutions. The matrix $\mathtt{C}$ will not be rank 3 if the conics were obtained by fitting to noisy image data. The above factorization truncates $\mathtt{C}$ to rank 3 by minimizing the error in the conic parameter space. Figure 3 shows the results of an implementation on synthetic data, leading to an accurately rectified house under low noise, but with reduced performance on more noisy data. Because the Frobenius norm minimization implied in the SVD solution to (13) does not minimize a geometric error in the image, this noise behaviour is predictable. In the following section we describe a method for computing $\mathtt{A}$ from noisy image data of straight lines in the real world.

4.1 Method for real image data

The overall strategy for fitting $\mathtt{A}$ from noisy image data is to run a non-linear optimization that finds the $\mathtt{A}$ which minimizes the error between the image data and straight lines projected (as conics) into the distorted image (see Figure 4). This requires a reasonable initialization of $\mathtt{A}$, knowledge of straight lines in the real world, and an error measure in the image plane.

A good initialization for $\mathtt{A}$ can be obtained using the parametrization of §3.1. We guessed that the field of view for our fish-eye lens is roughly 90° so $\omega = 0.5$.

The first task in finding straight lines is to detect curved line segments in the distorted image. Edgels are detected to subpixel accuracy using the Canny edge detector [5]. Adjacent edgels are then linked into curved segments $\mathbf{e} = e_1 \ldots e_L$ based on smoothly varying

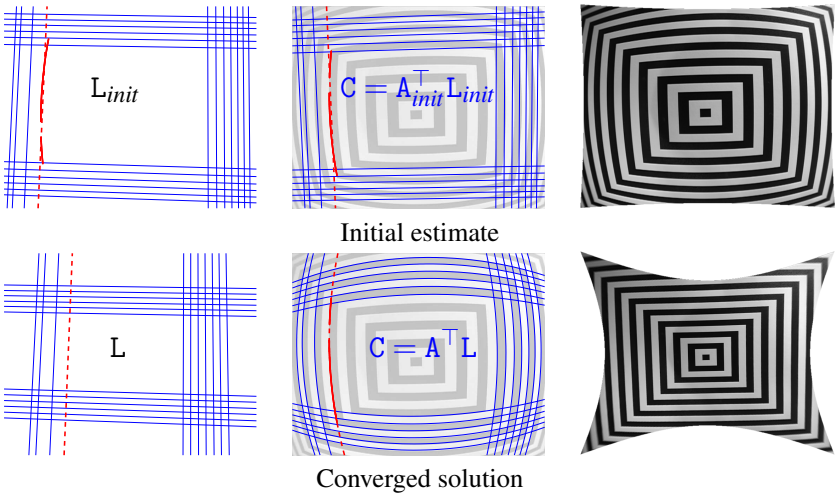

Figure 4: Non-linear optimization to fit A to the distorted images of straight lines. *Top (left to right)* The initial lines L are fit to edge data in the distorted image. These lines are projected into conics C in the distorted image via A. The image with distortion corrected via A. *Bottom* The optimization varies A and L to minimize the error measured between the edgels and the projected conics C.

edge orientations. The true orientation of the straight lines L in the world is not known, so they must be included in the optimization. An initial estimate is performed by fitting straight lines to the detected image edgels. The overall parametrization $(a, b, \omega, \mathbf{l}_1 \dots \mathbf{l}_L)$ is analogous to bundle adjustment [25] and the ellipse fitting approach of [10].

We then project the lines into conics in the image using (13) and measure the Sampson distance [19] from the conics to the detected edgels. The Sampson distance is a first order approximation to the distance from a point to a conic. Let $\mathbf{e}_{\ell k} = (i_{lk}, j_{lk})$ denote the k^{th} edgel in linked segment ℓ. The error function we minimize is then given by:

$$\sum_{\ell=1}^{L} \sum_{k=1}^{n_l} \left[\frac{\theta_\ell^\top \chi\,(i_{lk}, j_{lk})}{[(2A_{xx} i_{lk} + A_{xy} j_{lk} + A_x)^2 + (2A_{yy} j_{lk} + A_{xy} i_{lk} + A_y)^2]^{1/2}} \right]^2 . \tag{14}$$

We used MATLAB's lsqnonlin to perform the minimization. It is important to: 1) use the signed error (inside the square brackets in (14)); 2) pre-compute the lifted edgel coordinates; and 3) normalize the parameter vector so that all entries are in the range $[-1 \dots 1]$.

Note that this computes the error measured on detected edgels in the distorted image. After minimization using the reduced parametrization of §3.1, the full 18-parameter model can be fit nonlinearly.

4.2 Multiple views

The plumbline constraint obtained from edgels in one image is entirely independent of the camera's external calibration parameters, so repositioning the camera does not alter the *internal* calibration A. This enables us to combine constraints C obtained from M views in a single calibration:

Figure 5: Calibration from multiple views. Lines observed in separate views can be combined in a single calibration because $\mathtt{A}$ describes the *internal* properties of a camera. This rectification used only 14 lines (7 from each view).

$$[\mathtt{C}_1 \mid \ldots \mid \mathtt{C}_M] = \mathtt{A}^{\top} [\mathtt{L}_1 \mid \ldots \mid \mathtt{L}_M]. \tag{15}$$

These views may be of different scenes or even calibration grids; the only requirement is that there be straight lines visible and that the same camera be used. Figure 5 shows a calibration obtained from two views of a wrought iron fence.

5 Results and discussion

The calibration results for the sequences shown in Figures 1,4 and 5 are given in Table 1. The RF model yields subpixel calibration accuracy from one or two input images. Note that the optimization of §4.1 could be performed on all of the input edgels simultaneously to achieve a better fit. In Figure 4 the optimization was initialized with both $\omega = 0.001$ (pinhole camera, shown) and $\omega = 1$ (180° field of view); each converged to the same result, implying a wide basin of convergence. Convergence was also verified on synthetic data with a noise level of 2 pixels (Figure 3). The noise sensitivity of the linear factorization was explored by varying the noise level on the synthetic data; careful conditioning of the input data helps somewhat, but the calibration still fails to rectify above a noise level of 0.01 pixels.

In conclusion, we have shown how the rational function model permits an elegant formulation of the plumbline constraint, and have demonstrated camera calibration from a single view of straight lines. The simple form of the model (world lines expressed as image conics) accurately and succinctly represents the underlying camera properties. The model can be fit to noisy data by a nonlinear optimization which minimizes a geometric quantity in the image plane. The elegant linear factorization algorithm for calibration is

Sequence	Lines	Edgels	a	ω	Residual
Tower	21	5805	1.03	0.68	0.42
Grid	23	10 716	1.04	0.63	0.36
Fence	14	4574	1.06	0.70	0.62

Table 1: Summary of calibration results. The residual errors are the RMS Sampson distances from the edgels to the corresponding conics, measured in pixels. The initialization values were $a = 1.07$, $\omega = 0.5$, and b was fixed at 2×10^7. All images are 720×576.

more sensitive to noise because it lacks such a geometric constraint. This is an area of ongoing investigation.

References

[1] A. Basu and S. Licardie. Alternative models for fish-eye lenses. *Pattern Recognition Letters*, 16:433–441, 1995.

[2] P. A. Beardsley and D. W. Murray. Camera calibration using vanishing points. In *Proc. BMVC.*, pages 416–425. Springer-Verlag, 1992.

[3] H.A. Beyer. Accurate calibration of CCD cameras. In *Proc. CVPR*, pages 96–101, 1992.

[4] D.C. Brown. Close-range camera calibration. *Photogrammetric Engineering*, 37(8):855–866, 1971.

[5] J. F. Canny. A computational approach to edge detection. *IEEE PAMI*, 8(6):679–698, 1986.

[6] B. Caprile and V. Torre. Using vanishing points for camera calibration. *IJCV*, 4:127–140, 1990.

[7] D. Claus and A. W. Fitzgibbon. A rational function lens distortion model for general cameras. In *Proc. CVPR*, volume 1, pages 213–219, 2005.

[8] F. Devernay and O. Faugeras. Straight lines have to be straight. *Machine Vision Appl.*, 13:14–24, 2001.

[9] A. W. Fitzgibbon. Simultaneous linear estimation of multiple view geometry and lens distortion. In *Proc. CVPR*, volume 1, pages 125–132, 2001.

[10] W. Gander, G.H. Golub, and R. Strebel. Least-squares fitting of circles and ellipses. *BIT. Numerical Mathematics*, 34(4):558–578, 1994.

[11] C. Geyer and K. Daniilidis. Structure and motion from uncalibrated catadioptric views. In *Proc. CVPR*, volume 1, pages 279–286, 2001.

[12] R. I. Hartley and T. Saxena. The cubic rational polynomial camera model. In *Proc. DARPA Image Understanding Workshop*, pages 649–653, 1997.

[13] R. I. Hartley and A. Zisserman. *Multiple View Geometry in Computer Vision*. Cambridge University Press, ISBN: 0521623049, 2000.

[14] J. Heikkilä. Geometric camera calibration using circular control points. *PAMI*, 22(10):1066–1077, 2000.

[15] E. Kilpelä. Compensation of systematic errors of image and model coordinates. *International Archives of Photogrammetry*, XXIII(B9):407–427, 1980.

[16] B. Mičušík and T. Pajdla. Estimation of omnidirectional camera model from epipolar geometry. In *Proc. CVPR*, volume 1, pages 485–490, 2003.

[17] M.A. Penna. Camera calibration: A quick and easy way to determine the scale factor. *IEEE PAMI*, 13(12):1240–1245, 1991.

[18] R. Pless. Using many cameras as one. In *Proc. CVPR*, volume 2, pages 587–593, 2003.

[19] P. D. Sampson. Fitting conic sections to 'very scattered' data: An iterative refinement of the Bookstein algorithm. *Computer Vision, Graphics, and Image Processing*, 18:97–108, 1982.

[20] C. Slama. *Manual of Photogrammetry*. American Society of Photogrammetry, Falls Church, VA, USA, 4th edition, 1980.

[21] G. Stein. Lens distortion calibration using point correspondences. In *Proc. CVPR*, pages 602–608, 1997.

[22] P. Sturm and S. Ramalingam. A generic concept for camera calibration. In *Proc. ECCV*, volume 2, pages 1–13, 2004.

[23] R. Swaminathan and S. Nayar. Nonmetric calibration of wide-angle lenses and polycameras. *IEEE PAMI*, 22(10):1172–1178, 2000.

[24] V. Tao, Y. Hu, and W. Jiang. Photogrammetric exploitation of IKONOS imagery for mapping applications. *International Journal of Remote Sensing*, 25(14):2833–2853, 2004.

[25] W. Triggs, P. McLauchlan, R. Hartley, and A. Fitzgibbon. Bundle adjustment: A modern synthesis. In *Vision Algorithms: Theory and Practice*, LNCS 1883, pages 298–375. Springer Verlag, 2000.

[26] Y. R. Tsai. A versatile camera calibration technique for high-accuracy 3D machine vision metrology using off-the-shelf TV cameras and lenses. *Journal of Robotics and Automation*, RA-3(4):323–344, 1987.

[27] Z. Zhang. On the epipolar geometry between two images with lens distortion. In *Proc. ICPR*, pages 407–411, 1996.